Limit regimes of ice formation in turbulent supercooled water

Francesca De Santi and Piero Olla*
ISAC-CNR and INFN, Sez. Cagliari, I–09042 Monserrato, Italy
(Received 14 October 2016; published 10 October 2017)

A study of ice formation in stationary turbulent conditions is carried out in various limit regimes of crystal growth, supercooling, and ice entrainment at the water surface. Analytical expressions for the temperature, salinity, and ice concentration mean profiles are provided, and the role of fluctuations in ice production is numerically quantified. Lower bounds on the ratio of sensible heat flux to latent heat flux to the atmosphere are derived and their dependence on key parameters such as salt rejection in freezing and ice entrainment in the water column is elucidated.

DOI: 10.1103/PhysRevE.96.043106

I. INTRODUCTION

Ice production in polar oceans usually occurs in the presence of turbulence and wave motions induced by strong winds. This prevents the formation of a continuous ice layer at the sea surface in the initial phases (thin ice films, called nilas, are indeed observed in very calm conditions). A slurry of ice crystals, with a characteristic milky or greasy appearance, called grease ice, is generated instead. The ice crystals, called frazil crystals or frazil ice, have diameters ranging from 0.01 up to $\sim$4 mm and thickness from $1-100$ μm [1]. If the wind is sufficiently strong, the frazil ice may be blown away, leaving the water surface exposed to the cold air, thus enhancing the ice production and the heat transfer to the atmosphere [2]. Agglomeration of the frazil crystals first into pancake-shaped objects (so-called pancake ice [3]) and then into larger floes, leads eventually to the formation of a compact ice layer.

Frazil ice is typically present in the marginal ice zone, which is the transition region between the open polar ocean and the continuous ice that covers the central basin, but is also present under ice shelves, in polynyas, and in leads. Ice production is accompanied by salt rejection, and is thus believed to play an important role in stimulating convection in ocean waters. Frazil ice may also contribute to transport of nutrients and other trace elements entrained in its body [4,5].

Frazil ice formation is a complex phenomenon in which many physical processes play a relevant role [6]. We can list the most important ones.

(i) Small droplets and foam are continuously lifted up from the water surface and freeze in contact of the cold air. When they return to the water column they act as primary ice seeds.

(ii) If the upper layers of the ocean are sufficiently supercooled, ice crystals grow out of the seeds and reach size up to the millimeter range. New seeds are generated through fragmentation induced by collisions with other crystals (secondary nucleation).

(iii) Part of the crystals are entrained by the turbulence and are transported down the column. Additional ice production may take place away from the surface if the supercooling is sufficient. Field data indicate that underwater frazil ice and significant supercooling in the water column may indeed be present down to depths of 5–50 m (see, e.g., Ref. [7]).

Theoretical models for the growth and transport of frazil ice have been developed over the years. In the one-dimensional (1D) theory of Omstedt and Svensson [8], the upper ocean was modeled as a turbulent Ekman layer with the sea-ice mixture treated as a continuum. This model was improved in Refs. [9,10] to take into account the size spectrum of the crystals. Ice production under ice shelves was studied in Ref. [11], adopting a Boussinesq-like approximation. This latter study was later extended in Ref. [12] to account for the size spectrum of the frazil crystals. A detailed study of the precipitation of the frazil crystals on the shelf was carried out in Ref. [13]. The dynamics of frazil ice was included in regional ocean models [14]. Large eddy simulations (LES) were utilized in Ref. [15] to study the frazil ice dynamics under polar ice covers and leads, but no account was taken of the size distribution of the ice crystals. Only recently there has been some attempt to include such information in LES of frazil ice formation in open ocean [16].

Due to the complexity of the process, all these models necessarily rely on parametrization of small-scale phenomena and on the introduction of empirical constants. In such circumstances, it may be of some interest to look for limit regimes in which a reduced number of parameters is at play and identification of key physical aspects is simpler. This is precisely the strategy adopted in the present paper. The analysis will focus on the constraints imposed by the conservation laws and the thermodynamics of the process. The case of a homogeneous domain is examined first, analyzing the relative importance of salinity and heat release in ice formation in controlling supercooling. The analysis shifts then to the real problem, i.e., ice production in a water column that is mechanically forced and simultaneously cooled down at the top surface. Lower bounds on the ratio of sensible to total heat flux to the atmosphere, valid in stationary conditions, are derived. Predictions on the depth of the supercooled region and on the depth reached by frazil ice are provided.

II. ICE PRODUCTION: BUDGET EQUATIONS

Let us start by considering ice formation at constant pressure in a thermally isolated, initially supercooled volume of salt water. The water is stirred vigorously to maintain uniform conditions and to ensure that only small ice crystals are present. The volume is taken small enough for complications associated with differences between temperature and potential

*Corresponding author: olla@dsf.unica.it

temperature, and with the depth dependence of the freezing point, to be negligible.

We know that a variation δC in the volume fraction of ice leads to a heat release per unit volume in the liquid phase,

$$\delta Q^L = \mathcal{L}\rho_i \delta C, \tag{1}$$

where $\mathcal{L}$ is the latent heat of fusion per unit mass of ice and ρ_i is the ice density. This will produce a temperature increase in the liquid phase,

$$\delta T = (\hat{\rho}\mathcal{L}/c_P)\delta C, \tag{2}$$

where we have indicated with

$$\hat{\rho} = \rho_i/\rho_w \simeq 0.89 \tag{3}$$

the density ratio of ice and water, and c_P is the water specific heat (we consider a small C regime such that the ice contribution to the ice capacity of the medium is negligible; we also neglect the contribution to the heat flux from the temperature difference between the liquid phase and the ice [13], as it is much smaller than that from the latent heat).

During freezing a fraction $\beta \approx 1$ of the salt that was in the water forming the crystals is expelled to the surroundings [6]. The local salinity can be expressed as the sum of a reference salinity $S_R = 35$ g/kg and a deviation S that is expected in most situations to be small. A volume fraction increase δC in the ice thus corresponds to a decrease $\hat{\rho}\delta C$ of the liquid volume fraction, and to a release of salt per unit volume

$$\delta S = \hat{\rho}\beta S_R \delta C. \tag{4}$$

The water freezing temperature decreases for increasing pressure (depth) and salinity content. For small deviations, we have a linear relation [6]

$$T_i = -a_S S + a_z z, \tag{5}$$

where $-z$ is the depth and T_i is the deviation of the freezing temperature from the reference value $T_{iR} \simeq -2.09\,^\circ$C at salinity S_R and zero depth. Similarly, T will indicate from now on the deviation of the water temperature with respect to T_{iR}, i.e., the supercooling at salinity S_R and zero depth.

The decrease of the freezing point from creation of a volume fraction δC of ice is

$$\delta T_i = -\hat{\rho} a_S \beta S_R \delta C. \tag{6}$$

The supercooling in a water volume with initial supercooling $T_0 - T_{i0}$ and no ice, will be therefore, after formation of an ice volume fraction C,

$$T - T_i = T_0 - T_{i0} + (a_S \hat{S}_R + \hat{\mathcal{L}})C, \tag{7}$$

where

$$\hat{S}_R = \hat{\rho}\beta S_R \quad \text{and} \quad \hat{\mathcal{L}} = \hat{\rho}\mathcal{L}/c_P. \tag{8}$$

From Table I we find $a_S \hat{S}_R \simeq 1.76\ ^\circ$C and $\hat{\mathcal{L}} \simeq 75.5\ ^\circ$C. Warming from latent heat release is more effective in destroying supercooling than freezing point lowering by salinity increase. This implies that ice production can be sustained longer more effectively by cooling down the mass of water than by removing salt.

We can determine the ice volume fraction that can be generated starting from given supercooled condition by equating to zero the final supercooling $T - T_i$. From Eq. (7), we find

$$C_{\text{sat}} = \frac{T_{i0} - T_0}{\hat{\mathcal{L}} + a_S \hat{S}_R}. \tag{9}$$

For an initial supercooling $T_0 - T_{i0} = -0.1\ ^\circ$C of the order of what is observed in wave-tank experiments [17], and considered as maximum transient supercooling in several models (see, e.g., Refs. [10,15,16]), we would get an ice volume fraction at saturation $C_{\text{sat}} \simeq 0.0013$. Is it big or is it small? For a monodisperse suspension of disks of aspect ratio ϵ, the maximum volume fraction compatible with random orientation of the disks is $C \sim \epsilon$. This is what would be obtained if each volume of the fluid of size $\sim R^3$, with R the radius of the disks, contained on the average one disk. Higher volume fractions could be achieved (maintaining random orientation) if smaller crystals filled the gaps among the disks to form a mortarlike assembly. An estimate of the aspect ratio of typical frazil crystals is $\epsilon \approx 1/50$ [12,13], which would lead to a threshold volume fraction for grease ice $C_g \approx 1/50$. Higher volume fractions would correspond to more compact ice mixtures, with the transition to solid ice occurring at $C \approx 0.3$ [18]. Field measurements suggest a typical volume fraction of grease ice $C_g = 0.2$–0.3 [19,20]. Even the lower estimate $C_g \approx 1/50$ is an order of magnitude above the saturation concentration C_{sat} predicted by Eq. (9) at a supercooling $T - T_i \approx -0.1\ ^\circ$C. Transport of heat and salinity away from the production region, together with accumulation of the ice crystals, are therefore necessary for a grease ice layer to be established.

TABLE I. Physical parameters for salt water at reference temperature $T_B = -2.09\,^\circ$C, and total salinity $S_R = 35$ g/kg.

$a_S \simeq 0.0565\ ^\circ$C/(g/kg)	haline lowering of freezing point
$a_z \simeq 7.61 \times 10^{-4}\ ^\circ$C/m	lowering of freezing point with depth
$\alpha_T \simeq 3.79 \times 10^{-4}$ m/(°C s^2)	thermal buoyancy coefficient
$\alpha_S \simeq 7.6 \times 10^{-3}$ m/[(g/kg) s^2]	haline buoyancy coefficient
$\alpha_C \simeq 1$ m/s^2	ice buoyancy coefficient
$c_P \simeq 3947$ J/(kg °C)	water specific heat.
$\mathcal{L} \simeq 3.35 \times 10^5$ J/kg	specific latent heat of fusion.
$\rho_w \simeq 1030$ kg/m^3	reference water density.
$\rho_i \simeq 920$ kg/m^3	ice density.

III. TRANSPORT

We follow Refs. [8,13,15] and others, and coarse grain the dynamics at a scale such that the frazil ice can be treated as a continuum, described locally by the volume fraction field $C(\mathbf{r},t)$, which is supposed small throughout the analysis (for extension to a large C regime, see, e.g., Ref. [21]). Momentum transport is described by the Navier-Stokes equation, which in the Boussinesq approximation reads

$$(\partial_t + \mathbf{u}\cdot\nabla)\mathbf{u} + (1/\rho_w)\nabla P = \nu\nabla^2\mathbf{u} + (\alpha_T T + \alpha_C C - \alpha_S S)\hat{\mathbf{z}} \tag{10}$$

(we take the reference system with origin at the water surface, and the vertical z axis upward directed). The ice buoyancy coefficient can be expressed in terms of the ice density ratio as $\alpha_C = g(1-\hat{\rho}) \simeq 1$ m/s^2, where $g \simeq 9.8$ m/s^2 is the

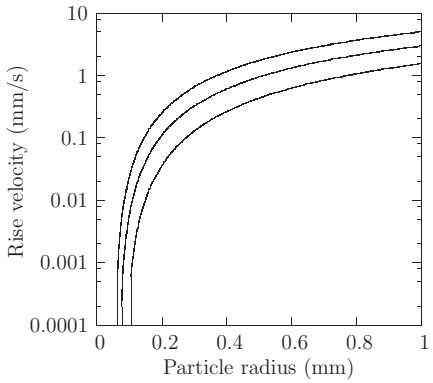

FIG. 1. Rise velocity u_r as a function of the particle radius for different values of the aspect ratio: $\epsilon = 1/100$ (bottom curve); $\epsilon = 1/50$ (middle curve); $\epsilon = 1/30$ (top curve).

gravitational acceleration. The values of the other coefficients α_T and α_S are listed in Table I. The kinematic viscosity of salt water is $\nu \simeq 1.95 \times 10^{-6}$ m^2/s.

We can determine the contribution to buoyancy that would be produced by a local increase δC in the ice volume fraction. Using Eqs. (2) and (4) to estimate the local increments of temperature and salinity:

$$\frac{\alpha_T \delta T}{\alpha_C \delta C} \approx 0.03, \quad \text{and} \quad \frac{\alpha_S \delta S}{\alpha_C \delta C} \approx 0.24. \tag{11}$$

This tells us that, while the dominant contribution to ice production saturation comes from latent heat release, the dominant contribution to convection comes directly from ice loading, followed by salinity.

The three fields T, S, and C are governed by equations (see, e.g., Ref. [8])

$$(\partial_t + \mathbf{u} \cdot \nabla) T = \kappa_T \nabla^2 T + \Pi_T, \tag{12}$$

$$(\partial_t + \mathbf{u} \cdot \nabla) S = \kappa_S \nabla^2 S + \Pi_S, \tag{13}$$

$$[\partial_t + (\mathbf{u} + \mathbf{u}_r) \cdot \nabla] C = \Pi_C, \tag{14}$$

where Π_T, Π_S, and Π_C are production terms whose form will be specified below.

The diffusivity coefficients in Eqs. (12) and (13) are $\kappa_T \simeq 1.4 \times 10^{-7}$ m^2/s, and $\kappa_S \simeq 7.4 \times 10^{-10}$ m^2/s, and the molecular diffusivity of the ice crystals is disregarded. Note that we have included in the equation for the ice fraction the rise velocity of the crystals relative to the surrounding water, $\mathbf{u}_r = u_r \hat{\mathbf{z}}$. This is necessarily an average, as crystals of different size and aspect ratio will have different rise velocity. Gosink and Osterkamp [22] provided model equations for u_r, in the case of individual crystals, as a function of their radius and thickness. A plot of such dependence is shown in Fig. 1.

The production terms can be taken in the form, from Eqs. (2) and (4):

$$\Pi_C = \Gamma C; \quad \Pi_S = \hat{S}_R \Gamma C; \quad \Pi_T = \hat{\mathcal{L}} \Gamma C. \tag{15}$$

Usually, a linear dependence of the growth rate Γ on the supercooling is assumed,

$$\Gamma = \gamma (T_i - T). \tag{16}$$

The parameter γ depends on the size distribution and the morphology of the crystals [23–25]. Some authors [11,13] hypothesize an asymmetry between melting and freezing rates, $\gamma_{T>T_i} \sim \epsilon^{-1} \gamma_{T<T_i}$. In general γ can be interpreted as the inverse time, normalized to the supercooling, required by a crystal to reach mature size. In the case of a monodisperse distribution, with aspect ratio of the crystals ϵ, γ can be evaluated, following Refs. [23–25]

$$\gamma \approx \hat{\gamma}/R^2, \qquad \hat{\gamma} = \hat{\gamma}(\epsilon). \tag{17}$$

Different authors provide different estimates for the parameter $\hat{\gamma}$. A widely used approximation [11,13,14] is the one from Ref. [24], $\hat{\gamma} \approx 3.7 \times 10^{-9}$ m^2(°C s)$^{-1}$; a value higher by a factor $\sim(\epsilon \ln \epsilon)^{-1}$ is suggested in Refs. [23,25], with experimental support for the latter choice in Ref. [26]. The two choices would give for frazil crystals of radius $R = 1$ mm and aspect ratio $\epsilon = 50$, $\gamma \approx 0.0037$ (°C s)$^{-1}$, and $\gamma \approx 0.04$ (°C s)$^{-1}$, respectively.

IV. A STATIONARY MODEL

It is likely that a significant portion of grease ice forms during an initial transient in which supercooling is strong [8]. After this, a quasistationary regime can be expected, although this is necessarily an idealization, since external conditions (say weather patterns) vary on the same time scale of the process itself. An approximation of statistical stationarity could nevertheless be used to describe the faster processes taking place near the water surface.

We envision a situation in which ice is formed primarily at the water surface. Part of this ice may be blown away by the wind, part of it accumulates at the surface to form a grease ice layer, and part of it is entrained in the water column. Additional ice formation may take place in the water column provided supercooling is sufficient. The depth of the supercooled region will depend on the ratio between the removal rate of frazil ice by turbulence and the rate of latent heat release during ice growth. The depth reached by the frazil ice will depend on the turbulence intensity, the rise velocity of the crystals, and the depth of the supercooled region. Whether and where such additional ice forms, however, is difficult to ascertain in field observations [7].

We consider the model situation of an infinitely deep, horizontally homogeneous water body cooled from above in stationary conditions. We assume that no ice is present at sufficient depth. This leads us to expect supercooling decreasing with depth both at the top of the column and in the ice-free region. We use these assumptions as boundary conditions in the ice production problem.

In the analysis that follows we disregard the pressure contribution to T_i [the $a_z z$ term in Eq. (5)]. For a supercooling scale $|T - T_i| \sim 0.1$ °C, this means restricting the analysis to the top few tens of meters of the physical water column.

Information on the way the heat, salinity, and frazil ice fluxes get organized in the domain can be obtained from simple budget considerations. Ice formation leads to a downward directed salinity flux in the ice-free region, Φ_S^B, and to a latent heat contribution to the heat flux to the atmosphere Φ_T^L. A schematic of the processes is illustrated in Fig. 2. From Eqs. (1) and (4), we can express the latent heat flux in terms

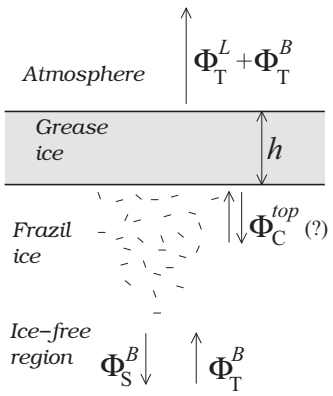

FIG. 2. Sketch of the heat, salinity, and ice fluxes generated during buildup of a grease ice layer. The heat flux to the atmosphere is split into latent heat Φ_T^L and sensible heat Φ_T^B contributions. The salinity flux Φ_S^B is downward directed. The question mark indicates that the sign of the frazil ice flux Φ_C^{top} is *a priori* undetermined.

of the salinity flux,

$$\Phi_T^L = -(\hat{\mathcal{L}}/\hat{S}_R)\Phi_S^B \tag{18}$$

(we express heat fluxes in units $^\circ$C m/s; conversion to natural units, W/m^2, is achieved by multiplication with $\rho_w c_P$). Putting together with the sensible heat flux Φ_T^B, which coincides with the total heat flux in the ice-free region, we get the total heat flux to the atmosphere

$$\Phi_T^{\rm tot} = \Phi_T^B - (\hat{\mathcal{L}}/\hat{S}_R)\Phi_S^B. \tag{19}$$

We can then introduce supercooling and neutral temperature fields (we focus on a condition in which the pressure contribution to T_i can be disregarded)

$$T_o = T + a_S S \tag{20}$$

and

$$T_n = T - (\hat{\mathcal{L}}/\hat{S}_R)S \tag{21}$$

(note that $T_o < 0$ in supercooled regions). As can be checked from Eqs. (12) and (13), T_o and T_n are decoupled, with only T_o feeling the effect of ice formation and melting. The flux $\Phi_{T_n} = \Phi_T - (\hat{\mathcal{L}}/\hat{S}_R)\Phi_S$ is therefore conserved. We find from Eq. (19),

$$\Phi_{T_n} = \Phi_T^{\rm tot}. \tag{22}$$

The temperature and salinity contributions to buoyancy can be expressed in terms of the fields $T_{o,n}$: $T - (\alpha_S/\alpha_T)S \simeq$ const. $- 8.05\, T_o + 9.05\, T_n$. We note that fixed T_n, a supercooled condition at large depth, will be less stable than one in which the bottom is above freezing.

The condition $\partial_z \bar{T}_o^B < 0$ leads to the requirement that the supercooling flux in the ice-free region is upward directed [27]

$$\Phi_{T_o}^B \equiv \Phi_T^B + a_S \Phi_S^B > 0. \tag{23}$$

Equation (23) tells us that the ratio $\mathcal{B} = \Phi_T^B/\Phi_T^{\rm tot}$ of sensible to total heat flux cannot be zero, the minimum value being

$$\mathcal{B}_{\rm min} = \frac{a_S \hat{S}_R}{\hat{\mathcal{L}} + a_S \hat{S}_R}. \tag{24}$$

From Eq. (8), $\mathcal{B}_{\rm min}$ is an increasing function of the brine release coefficient β and is maximum for $\beta = 1$, $\mathcal{B}_{\rm min} \simeq 0.025$. The smallness of $\mathcal{B}_{\rm min}$ has origin in the smallness of the contribution to supercooling destruction from salinity release with respect to latent heat release in ice formation [see Eqs. (7) and (8) and following discussion]. The maximum value $\mathcal{B} = 1$ describes a situation in which $\Phi_T^L = 0$ and there is exact balance between ice production and melting.

A. Frazil ice fluxes in the water column

Frazil ice in the water column acts as a sink term for the supercooling field T_o. Equations (2) and (4) yield conservation of the flux

$$\Phi_{\mathcal{X}} = \Phi_{T_o} - (\hat{\mathcal{L}} + a_S \hat{S}_R)\Phi_C, \tag{25}$$

which is associated with the field

$$\mathcal{X} = T_o - (\hat{\mathcal{L}} + a_S \hat{S}_R)C. \tag{26}$$

A formula analogous to Eq. (22) can be derived,

$$\Phi_{\mathcal{X}} = \Phi_{T_o}^B. \tag{27}$$

As in the case of T_n, the field $\mathcal{X}$ is not affected by ice production.

The frazil ice flux Φ_C in the water column is the sum of the contributions by deposition and turbulent entrainment,

$$\Phi_C = \bar{C} u_r + \overline{\tilde{u}_z \tilde{C}} \tag{28}$$

(overbar and tilde indicate average and fluctuating components). The flux on the top of the column, $\Phi_C^{\rm top}$, will be positive if deposition $\bar{C}u_r$ dominates. At stationarity, positive $\Phi_C^{\rm top}$ necessarily corresponds to ice production exceeding melting in the water column.

Let us introduce the ratio $\mathcal{E}$ of the frazil flux at the top of the column, taken with minus sign, $-\Phi_C^{\rm top}$, and the total ice production $\Phi_T^L/\hat{\mathcal{L}}$. The two regimes $\mathcal{E} > 0$ and $\mathcal{E} < 0$ describe dominant entrainment and dominant deposition, respectively. In terms of the parameter $\mathcal{B}$,

$$\Phi_C^{\rm top} = (\mathcal{E}/\hat{\mathcal{L}})(\mathcal{B} - 1)\Phi_T^{\rm tot}. \tag{29}$$

Note, from positive definiteness of the deposition flux, that we must have $\mathcal{E} \leqslant 1$.

The assumption $\partial_z \bar{T}_o^{\rm top} < 0$ allows us to refine the bound in Eq. (24). From Eq. (25) and the condition that no ice is present at large depth, we find

$$\Phi_{T_o}^{\rm top} = \Phi_{T_o}^B + (\hat{\mathcal{L}} + a_S \hat{S}_R)\Phi_C^{\rm top} > 0. \tag{30}$$

The salinity flux in the ice-free region, Φ_S^B, can be expressed in terms of the latent heat flux $\Phi_T^{\rm tot} - \Phi_T^B = \Phi_{T_n} - \Phi_T^B$: $\Phi_S^B = (\hat{S}_R/\mathcal{L})(\Phi_T^B - \Phi_{T_n})$. Substituting into the supercooling and neutral fluxes in the ice-free region, $\Phi_{T_o}^B = \Phi_T^B + a_S \Phi_S^B$ and $\Phi_{T_n} = \Phi_T^B - (\hat{\mathcal{L}}/\hat{S}_R)\Phi_S^B$, and eliminating Φ_T^B, allows us to write

$$\Phi_{T_n} = \frac{1 - \mathcal{B}_{\rm min}}{\mathcal{B} - \mathcal{B}_{\rm min}} \Phi_{T_o}^B, \tag{31}$$

where use has been made of Eqs. (22) and (24). Substituting into Eq. (30) and exploiting Eq. (29) finally gives

$$\mathcal{B} > \bar{\mathcal{B}}_{\min}(\mathcal{E}) = \frac{\mathcal{B}_{\min} + \mathcal{E}}{1 + \mathcal{E}}. \tag{32}$$

In the limit $\mathcal{B} \to \bar{\mathcal{B}}_{\min}(\mathcal{E})$, all of the supercooling flux $\Phi^B_{T_o}$ is utilized to melt the frazil ice in the column, and $\Phi^{\text{top}}_{T_o} = 0$. For $\mathcal{E} = 0$ (balance of entrainment and deposition), we recover the bound in Eq. (24). The same situation occurs for $\mathcal{E} < 0$ (deposition dominant with respect to entrainment), in which case the bound in Eq. (24) becomes stronger than the one in Eq. (32). In the limit case in which all the ice is entrained in the column, the sensible heat flux must be at least a fraction $\bar{\mathcal{B}}_{\min}(1) \simeq 1/2$ of the total heat flux.

V. GREASE ICE LAYER

In order for ice production to be maintained in the grease ice layer—if at all present—it is necessary that the salt released in the process is efficiently transported down the layer and dispersed in the water column. Due to the high viscosity of the medium ($\nu_g \simeq 0.01$ m^2/s [28]), turbulent transport is negligible. Wave-induced random motions at the scale of the ice crystals, however, are likely to enhance transport with respect to the case of a pure fluid in analogous conditions. Some analytical progress is possible if we assume that this is the dominant mechanism of transport, with identical diffusivity for heat and salinity $\kappa_g \gg \kappa_{T,S}$.

The transport equations derived in Sec. III can be extended to the finite C conditions characteristic of grease ice. We continue to assume stationary conditions, in such a way that all the heat produced during ice formation is transferred to the liquid phase and carried away by diffusion. Equations (12) and (13) become

$$\partial_z(\kappa_g \partial_z \bar{T}) + \hat{\mathcal{L}}\Gamma\bar{C} = 0, \tag{33}$$

$$\partial_z(\kappa_g \partial_z \bar{S}) + \hat{S}_R\Gamma\bar{C} = 0, \tag{34}$$

where $\bar{T}$ and $\bar{S}$ refer to the liquid phase and a volume factor $1 - \bar{C}$ is incorporated in κ_g.

The rate of ice formation is determined by the removal of heat and salt in the region around the crystals. We expect that the equations governing transport at the microscale be linear in T and S [29], so that for small T_o, $\Gamma \approx -\gamma_g T_o$, with γ_g a constant dependent on C and on the crystal geometry. We can obtain from Eqs. (33) and (34), equations for T_o and T_n:

$$\partial_z(\kappa_g \partial_z \bar{T}_o) = \hat{\mathcal{L}}\gamma_g \bar{C}\bar{T}_o \quad \text{and} \quad \partial_z(\kappa_g \partial_z \bar{T}_n) = 0. \tag{35}$$

We identify in the first of Eq. (35) a characteristic length

$$l \approx \left(\frac{\kappa_g}{\gamma_g \hat{\mathcal{L}}\bar{C}}\right)^{1/2}, \tag{36}$$

which we allow to depend on z on scale h. We can make some estimates from parameters valid in the dilute regime. Taking $\gamma_g \approx 0.04$ (°C s)$^{-1}$, and $\bar{C} \approx 0.2$, we obtain l values ranging from millimeters (for $\kappa_g \approx \kappa_T$) to tens of centimeters (for $\kappa_g \approx \nu_g \approx 0.01$ m/s^2).

Of the two relevant limits $l \ll h$ and $l \gg h$, only the first is of some interest. For $l \gg h$, it is easy to see by Taylor expanding Eq. (35), that ice production in the grease ice layer contributes to the heat flux with an $O(h/l)$ correction, so that, in the absence of ice formation in the water column, $\mathcal{B} \simeq 1$. The interest of the opposite limit regime $l \ll h$ lies in the fact that it allows an easier interpretation of the lower bound in Eq. (24). Let us consider first the case $\bar{T}(-h) = 0$ (no ice formation or melting at the bottom of the layer).

Equation (35) has solution, for $z \gg -h$,

$$\bar{T}_o(z) = \bar{T}_o(0)\, e^{z/l_0} + \mathcal{T}(e^{-z/l} - e^{z/l_0}), \tag{37}$$

$$\bar{T}_n(z) = \bar{T}_n(0) + \bar{T}'_n z, \tag{38}$$

where $l_0 \equiv l(0)$. In the regime $l \ll h$, $\mathcal{T} \simeq -\bar{T}_o(0)\exp[-2\int_{-h}^{0} dz/l(z)] \simeq 0$, and the second constant T'_n in Eq. (38), is fixed by imposing that there is no salt flux to the atmosphere, $\bar{S}'(0) = 0$. This gives

$$\bar{T}'_n = \bar{T}_o(0)/l_0. \tag{39}$$

The fact that there is no supercooling at $-l \gg z \gg -h$, $\bar{T}_o(z) = 0$, implies that temperature and salinity are dominated by $\bar{T}_n$ and have a linear profile [see Eq. (38)]. We can calculate the heat and salinity fluxes $\Phi_T = -\kappa_g \bar{T}'$ and $\Phi_S = -\kappa_g \bar{S}'$ in this region. Substituting Eq. (39) and the condition $\bar{T}_o(z \ll -l) = 0$ into Eqs. (20) and (21), we get

$$\Phi_T = -\kappa_g \mathcal{B}_{\min} \bar{T}_o(0)/l_0; \tag{40}$$

$$\Phi_S = (1 - \mathcal{B}_{\min})\kappa_g \hat{S}_R \bar{T}_o(0)/(\hat{\mathcal{L}} l_0). \tag{41}$$

Since $\bar{T}_o(-h) = 0$, there will be no melting at the bottom surface and the heat flux right below will still be given by Eq. (40). If the water in that region is ice free, the heat flux will coincide with the sensible heat flux Φ^B_T and by exploiting (39) and (22) we obtain $\Phi^B_T = \mathcal{B}_{\min}\Phi^{\text{tot}}_T$. Thus $\mathcal{B} = \mathcal{B}_{\min}$ and the latent heat contribution to the heat flux to the atmosphere is maximum. A situation in which $\mathcal{B} > \mathcal{B}_{\min}$ corresponds to ice melting at the bottom of the layer, with the difference $(\mathcal{B} - \mathcal{B}_{\min})\Phi^{\text{tot}}_T$ giving precisely the heat required for melting. The same situation would arise if $\bar{T}_o$ remained close to zero at $z = -h$, but frazil ice was entrained by turbulence and melted down upon reaching the region with $\bar{T}_o > 0$ at the bottom of the column. The interpretation of $(\mathcal{B} - \mathcal{B}_{\min})\Phi^{\text{tot}}_T$ as a melting heat is clearly lost if the grease ice is so thin that it loses its insulating properties and the excess heat is transferred to the atmosphere.

VI. WATER COLUMN

Frazil ice production requires strong winds. A minimum wind velocity $u_{\text{wind}} = 4.35$ m/s at 10 m above the water surface was suggested in Ref. [20] as a necessary condition for frazil ice formation. A turbulent boundary layer forced both by mechanical stress and convection induced by heat and salinity fluxes is thus expected to exist below the grease ice layer.

An estimate of the friction velocity u_* generated under the water surface by the wind stress was provided in Ref. [20],

$$u_* \approx A[\hat{\rho}_{\text{air}}(1 + u_{\text{wind}}/\bar{u})]^{1/2} u_{\text{wind}}, \tag{42}$$

where $\hat{\rho}_{\rm air} \approx 10^{-3}$ is the air water density ratio, and A and $\bar{u}$ are empirical constants: $A = 0.028$ and $\bar{u} = 12.3$ m/s. A ten-meter wind velocity $u_{\rm wind} = 10$ m/s would lead to a friction velocity

$$u_* \approx 0.01 \text{ m/s}. \tag{43}$$

The strength of the convective forcing can be estimated from the heat flux to the atmosphere. Estimates of the heat flux during frazil ice production events fall in the range

$$\Phi_T^{\rm tot} = 2.5 \times 10^{-5}\text{–}10^{-4} \,^\circ\text{C m/s}, \tag{44}$$

corresponding in energy units to $\rho_w c_P \Phi_T^{\rm tot} = 100$–$1000\,\text{W/m}^2$ [8,16,20]. From Eqs. (43) and (19) we can define an Obukhov depth signaling transition from a mechanical stress dominated to a thermal convection dominated turbulent region

$$L_T = \frac{u_*^3}{\alpha_T \Phi_T^{\rm tot}} = 10\text{–}100 \text{ m} \tag{45}$$

(this is clearly a lower bound since the heat flux responsible for convection is only a fraction of Φ_T). The Obukhov depth is going to be reduced by salt release in ice formation. If all the heat ceded to the atmosphere came from ice formation we would get

$$L_S = \frac{\hat{\mathcal{L}} u_*^3}{\alpha_S \hat{S}_R \Phi_T^{\rm tot}} = 1\text{–}10\,\text{m}, \tag{46}$$

which tells us that already $1/10$ of $\Phi_T^{\rm tot}$ coming from ice formation would be sufficient to invalidate Eq. (45). The estimate in Eq. (46) would be further reduced if ice were transported down the column together with the brine,

$$L_C = \frac{\hat{\mathcal{L}} u_*^3}{\alpha_C \Phi_T^{\rm tot}} = 0.3\text{–}3\,\text{m}. \tag{47}$$

Note, from the second of Eq. (11), that transport down the column of just $1/4$ of the ice produced at the surface, would be sufficient to counterbalance the destabilizing effect of salinity production.

VII. TURBULENT BOUNDARY LAYER

We assume that a well-developed mechanical boundary layer, in which the feedback by C, T_o, and T_n on the turbulence can be disregarded, exists. We focus on a low-entrainment regime, $\mathcal{E} \ll 1$, such that the depth of the boundary layer is correctly estimated by L_S. The friction velocity u_* and the Obukhov length L_S provide the natural scales for the velocity fluctuations in that region. A natural scale for the reacting fields C and T_o is the supercooling flux in the ice-free region, $\Phi_{T_o}^B \equiv \Phi_{\mathcal{X}}$.

We rescale quantities in terms of L_S, u_*, and $\Phi_{\mathcal{X}}$:

$$\begin{aligned} &z \to L_S z, \quad t \to (L_S/u_*)t, T_{o,n} \to (\Phi_{\mathcal{X}}/u_*)T_{o,n}, \\ &C \to [u_*(\hat{\mathcal{L}} + a_S \hat{S}_R)]^{-1} \Phi_{\mathcal{X}} C. \end{aligned} \tag{48}$$

After rescaling, $\mathcal{X} = T_o - C$. It is convenient to introduce the reacting field

$$\mathcal{Y} = T_o + C. \tag{49}$$

The ice dynamics is simplified considering that only crystals with $u_R \ll u_*$ are transported down the column (we are not interested here in the determination of the deposition fluxes at the surface, which would require studying the dynamics of the crystal size spectrum). We thus neglect u_r in Eq. (14). Transport in a horizontally homogeneous mechanical boundary layer can be modeled by introducing an eddy diffusivity $\kappa_{\rm turb} \approx -\sigma u_* z$, where $\sigma = 0.4$ is the von Karman constant (we neglect all sources of inhomogeneity, such as Langmuir turbulence [30]). Transport equations in dimensionless form for the fields T_n, $\mathcal{X}$, and $\mathcal{Y}$ can be obtained from Eqs. (12)–(14) by replacing the advection terms with an eddy diffusion. Exploiting Eqs. (27), (24), and (46) allows to eliminate any explicit dependence on the heat fluxes. We get

$$\partial_z(z\partial_z \bar{\mathcal{Y}}) + (1/2)[\overline{\lambda \mathcal{Y}^2} - \overline{\lambda \mathcal{X}^2}] = 0, \tag{50}$$

$$\partial_z(z\partial_z \bar{T}_n) = \partial_z(z\partial_z \bar{\mathcal{X}}) = 0, \tag{51}$$

where

$$\lambda = \frac{H_{\mathcal{B}} u_* \gamma \hat{\mathcal{L}}}{\sigma \alpha_S \hat{S}_R}, \tag{52}$$

with $H_{\mathcal{B}} = (\mathcal{B} - \mathcal{B}_{\rm min})/(1 - \mathcal{B}_{\rm min})$, gives the relative strength of the contributions to the dynamics from ice formation and transport. The parameter λ could equivalently be seen as the ratio of the turbulent transport time scale L_S/u_* and the reaction time scale $u_*/(\Phi_{T_o}^{\mathcal{B}}\gamma)$, which explains the counterintuitive proportionality with u_*. It is interesting to note that λ vanishes in the limit $\mathcal{B} \to \mathcal{B}_{\rm min}$, corresponding to the limit $\mathcal{E} \to 0$ in Eq. (32). Note that we allow in Eq. (50) for the possibility of fluctuations in λ, which would develop in the case of dependence of γ on the sign of T_o (see discussion at the end of Sec. III).

We can make some estimates. Assume turbulence strength $u_* \approx 0.01$ m/s and one-mm crystals with $\epsilon = 1/50$. The two estimates $\gamma \approx 0.0037\,(^\circ\text{C s})^{-1}$ [23,25] and $\gamma \approx 0.04\,(^\circ\text{C s})^{-1}$ [24] give $\lambda \approx 3H_{\mathcal{B}}$ and $\lambda \approx 0.3H_{\mathcal{B}}$, respectively. Smaller crystals lead to larger values of λ, but the effect is counteracted, at least in part, by the fact that such crystals typically have larger ϵ [31]. In general, λ is not small and the nonlinearity in Eq. (50) cannot *a priori* be disregarded.

We see from Eq. (51) that the two nonreacting fields T_n and $\mathcal{X}$ obey logarithmic scaling

$$\bar{T}_n(z) = \frac{1}{\sigma}\frac{1 - \mathcal{B}_{\rm min}}{\mathcal{B} - \mathcal{B}_{\rm min}} \ln(-z/\Lambda_n), \tag{53}$$

and

$$\bar{\mathcal{X}}(z) = (1/\sigma)\ln(-z/\Lambda_{\mathcal{X}}), \tag{54}$$

where the factors in front of the logarithms are $(1/\sigma)$ times the fluxes Φ_{T_n} and $\Phi_{\mathcal{X}}$ expressed in dimensionless form [see Eqs. (25), (31), and (48)], and $\Lambda_{n,\mathcal{X}}$ are free parameters determined by the asymptotic large depth behavior of the fields $\bar{T}$ and $\bar{S}$ (and $\bar{C}$ if it reaches the bottom of the layer).

The two limit regimes $\Lambda_n \ll 1$ and $\Lambda_n \gtrsim 1$, correspond to $\bar{T}_n > 0$ and $\bar{T}_n < 0$, respectively, in most of the domain. In the same way, $\Lambda_{\mathcal{X}} \ll 1$ and $\Lambda_{\mathcal{X}} \gtrsim 1$ correspond to $\bar{\mathcal{X}} > 0$ and $\bar{\mathcal{X}} < 0$ in most of the domain. For $\Lambda_{\mathcal{X}} \ll 1$, from positive

definiteness of C, most of the domain will be above freezing; for $\Lambda_{\mathcal{X}} \gtrsim 1$, either supercooling, or ice, or both will be present.

A. Two limit regimes

For small λ, the dynamics of $\mathcal{Y}$ in the mechanical boundary layer reduces to that of a passive scalar; $\mathcal{Y}$ and therefore also T_o and C obey in the first approximation logarithmic scaling.

For $\lambda \gtrsim 1$, solution of Eq. (50) is complicated by nonlinearity and by the presence of fluctuations. To make analytical progress, we momentarily neglect fluctuations. We can linearize the dynamics when either $\bar{C}$ or $\bar{T}_o$ are small.

Small $\bar{C}$ corresponds to a regime of small entrainment on the scale of T_o and above freezing conditions: $\Phi_C^{\rm top} \ll 1$, $\bar{T}_o > 0$. In this case, $\bar{T}_o \simeq \bar{\mathcal{X}}$ and the domain of interest is $\Lambda_{\mathcal{X}} \ll -z$. This corresponds to studying the melting dynamics of $\bar{C}$ for fixed $\bar{T}_o > 0$.

Small $\bar{T}_o$ corresponds to a regime in which large amounts of frazil ice are present in the column. In this case $\bar{C} \simeq -\bar{\mathcal{X}}$ and the domain of interest is $-z \ll \Lambda_{\mathcal{X}}$ (note that the frazil ice may reach the bottom of the mechanical boundary layer). This corresponds to studying the decay of $\bar{T}_o$ induced by ice formation or melting for fixed $\bar{C}$.

For small $\bar{C}$ we can approximate $\bar{\mathcal{Y}}^2 - \bar{\mathcal{X}}^2 = 4\bar{C}\bar{T}_o \simeq 4\bar{\mathcal{X}}\bar{C}$ and Eq. (54) becomes, exploiting Eqs. (51) and (54),

$$\sigma\,\partial_z(z\partial_z\bar{C}) + \bar{\lambda}\bar{C}\ln(-z/\Lambda_{\mathcal{X}}) = 0. \tag{55}$$

For small $\bar{T}_o$ we can approximate $\bar{\mathcal{Y}}^2 - \bar{\mathcal{X}}^2 = 4\bar{C}\bar{T}_o \simeq -4\bar{\mathcal{X}}\bar{T}_o$ and Eq. (54) becomes, exploiting again Eqs. (51) and (54),

$$\sigma\,\partial_z(z\partial_z\bar{T}_o) - \bar{\lambda}\bar{T}_o\ln(-z/\Lambda_{\mathcal{X}}) = 0. \tag{56}$$

The logarithm on the right-hand side of Eq. (55) gives the profile of $\bar{T}_o$, with $-z = \Lambda_{\mathcal{X}}$ the depth of the supercooled region; in Eq. (56), the logarithm gives the profile of $-\bar{C}$, with $-z = \Lambda_{\mathcal{X}}$ the maximum depth reached by the frazil ice.

Equations (55) and (56) are identical in form and describe decay (within logarithms) at depth $-z \sim \bar{\lambda}^{-1}$ of the respective field (note the minus sign in Eq. (56), which cancels the negative sign of the logarithm in the region $-z < \Lambda_{\mathcal{X}}$). Let us calculate the decay explicitly. We assume that decay takes place in the region of applicability of Eqs. (55) and (56), that is, the mechanical boundary layer $-z < 1$.

Consider first the case of Eq. (55), in which $\bar{C}$ is small and $\bar{T}_o \simeq \bar{\mathcal{X}}$. The singularity at $z \to -\infty$ in Eq. (55) is treated by working in the eikonal representation, $\bar{C} = \exp(W)$ [32]. To leading order in z, Eq. (55) becomes

$$\sigma z(W')^2 + \bar{\lambda}\ln(-z/\Lambda_{\mathcal{X}}) = 0, \tag{57}$$

which has solution, for $-z \gg \Lambda_{\mathcal{X}}$,

$$W(z) = \pm 2\sqrt{(-z\bar{\lambda}/\sigma)\ln(-z/\Lambda_{\mathcal{X}})}. \tag{58}$$

We get the asymptotic behavior

$$\bar{C}(z) \sim \exp\left[-2\sqrt{(-z\bar{\lambda}/\sigma)\ln(-z/\Lambda_{\mathcal{X}})}\right], \tag{59}$$

which leads to the decay depth for $\bar{C}(z)$

$$-z_C \sim |\bar{\lambda}\ln(\bar{\lambda}\Lambda_{\mathcal{X}})|^{-1}. \tag{60}$$

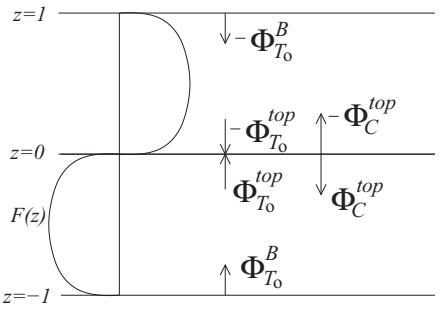

FIG. 3. Sketch of the computation domain.

The case in which $\bar{T}_o$ is small and $\bar{C} \simeq -\bar{\mathcal{X}}$ is treated in exactly the same way. We proceed with Eq. (56) as with Eq. (55), except that now $-z \ll \Lambda_{\mathcal{X}}$. We obtain for $\bar{T}_o(z)$ the same decay law in Eq. (60), $-z_{T_o} \sim |\bar{\lambda}\ln(\bar{\lambda}\Lambda_{\mathcal{X}})|^{-1}$.

VIII. FLUCTUATIONS

We estimate fluctuations in the mechanical boundary layer by means of a simple Kraichnan model [33,34], in a periodic 2D domain $[-1,1]\times[-1,1]$. We focus on the dynamics of the reacting fields T_o and C. We take x and z as the horizontal and vertical coordinates, with $z = 0$ the water surface and the periodic point $z = \pm 1$ the bottom of the boundary layer ($z = -L_S$ in the original units). The computation domain is thus split in two statistically equivalent mirror subdomains at $-1 < z < 0$ and $0 < z < 1$. The situation is illustrated in Fig. 3. We continue to work with the dimensionless variables defined in Eq. (48).

A boundary layer structure is imposed on the velocity fluctuations by means of a shape function $F = F(z)$. We write

$$u_x = \bar{u}_x - \partial_z\psi_F, \qquad u_z = \partial_x\psi_F, \tag{61}$$

where $\psi_F(\mathbf{r},t) = F(z)\psi(\mathbf{r},t)$ and $\psi(\mathbf{r},t)$ is zero mean, spatially homogeneous, and white in time,

$$\overline{\psi(\mathbf{r},t)\psi(\mathbf{r}',t')} = \Psi(\mathbf{r}-\mathbf{r}')\delta(t-t'). \tag{62}$$

We take for the shape function

$$F = \prod_{m\in\mathbb{Z}} \tanh[2\pi(z+m)] \tag{63}$$

and for $\bar{u}_x(z)$ a sum of logarithms mimicking the mean velocity profile in a turbulent channel flow.

We chose the shape function in such a way that $u_z(0) = 0$ but $u_x(0) \neq 0$, as expected for the turbulent velocity at the free water surface. The fact that $F'(0) \neq 0$, together with periodicity, require, however, that $F = 0$ and therefore $u_z = 0$ somewhere else in the domain. The choice $F(\pm 1) = 0$ is the one that less affects the dynamics, although it somewhat spoils the interpretation of $z = \pm 1$ as the bottom of the mechanical boundary layer.

We take for the spectrum $\Psi_{\mathbf{k}} = \int d^2r\, e^{-i\mathbf{k}\cdot\mathbf{r}}\Psi(\mathbf{r})$,

$$\Psi_{\mathbf{k}} = A\left(k^2 + k_0^2\right)^{-8/3}, \tag{64}$$

which guarantees Richardson scaling for relative diffusion at small separation [34]. The parameter k_0 is a large-scale cutoff that we put equal to 5π. The constant A is fixed by imposing

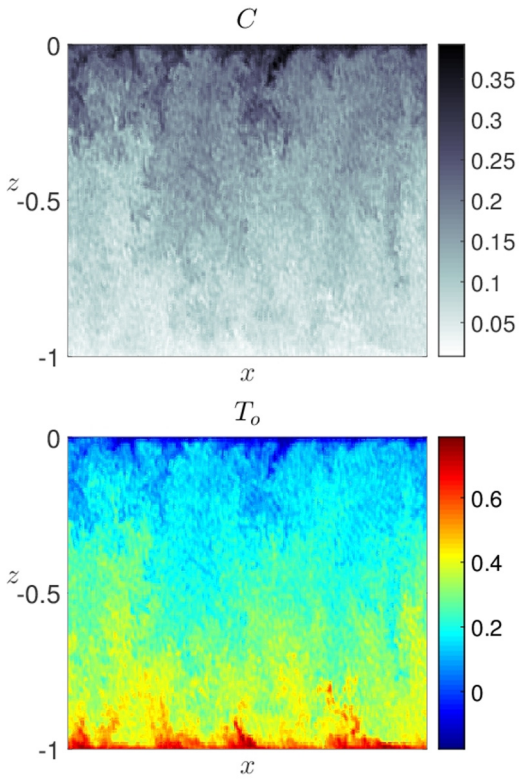

FIG. 4. Snapshot of the ice concentration (top) and the supercooling (bottom) for $\langle \mathcal{X} \rangle = -\Phi_C^{\text{top}} = 0.1$, $\lambda_- = 1$, and $\epsilon = 1/5$.

the condition for the spatial average of the turbulent diffusivity

$$\langle \kappa_{\text{turb}} \rangle = \int dt \, \langle \overline{u_z(\mathbf{r},t) u_z(\mathbf{r},0)} \rangle = 1, \tag{65}$$

which replaces the normalization $u_* = 1$ implicit in Eq. (48).

The presence of input and output fluxes for C and T_o at the boundaries of a periodic domain is mimicked introducing forcing terms at $z = 0$ and $z = -1$ in the transport equations (see Fig. 3). From Eqs. (12)–(14) and (48), we find (with z mod. 2):

$$(\partial_t + \mathbf{u} \cdot \boldsymbol{\nabla}) T_o = \kappa \nabla^2 T_o - \lambda C T_o + 2\big[- \big(\Phi_C^{\text{top}} + 1\big)\delta(z) + \delta(z+1)\big], \tag{66}$$

$$[\partial_t + (\mathbf{u} + \mathbf{u}_r) \cdot \boldsymbol{\nabla}] C = \kappa \nabla^2 C - \lambda C T_o - 2\Phi_C^{\text{top}} \delta(z), \tag{67}$$

where κ is understood as the turbulent diffusivity of the unresolved eddies below the spatial discretization scale and we recall, in dimensionless units, $\Phi_{T_o}^B = 1$, $\Phi_{T_o}^{\text{top}} = 1 + \Phi_C^{\text{top}}$.

Taking the difference of Eqs. (66) and (67), we see that the spatial average of $\mathcal{X} = T_o - C$ is conserved, $(d/dt)\langle \mathcal{X} \rangle = 0$, which is equivalent to the statement on conservation of $\Phi_{\mathcal{X}}$ in the previous section.

We solve numerically the system of equations (66)–(67), by means of a pseudospectral code on a 256×256 grid, taking $\kappa = 10^{-3}$. We smooth the white noise in Eq. (62) by replacing the Fourier modes $\psi_{\mathbf{k}}(t)$ with an Ornstein-Uhlenbeck processes with correlation time below the diffusion time at the discretization scale. An Adam-Bashford integration scheme

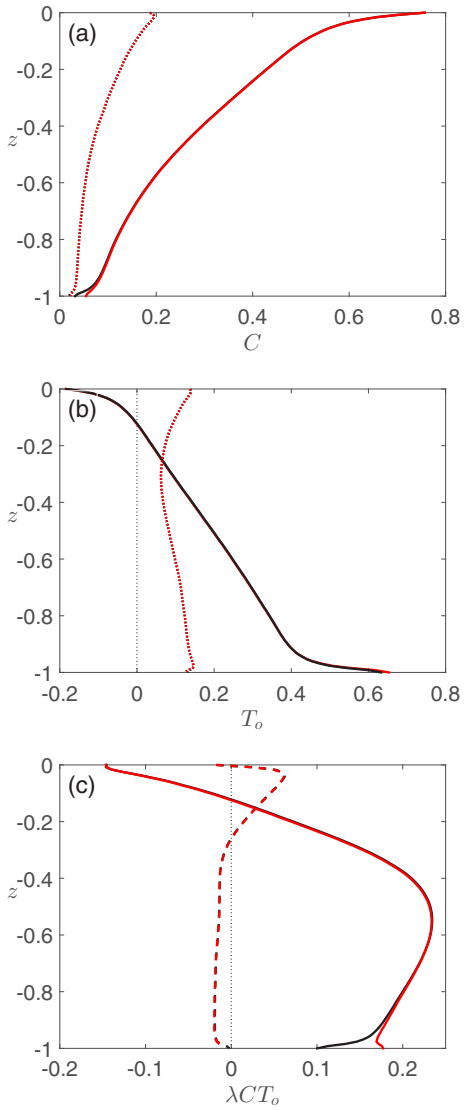

FIG. 5. Effect of an ice sink at $z = \pm 1$ on the vertical profiles of (a) ice concentration, (b) supercooling, and (c) ice production rate; $\Phi_C^B = 0$ in red; $\Phi_C^B = -0.3$ in black. In (a) and (b), solid lines indicate average; in (c), they indicate mean-field result $\bar{\lambda}\bar{C}\bar{T}_o$. In (a) and (b), dashed line indicate rms; in (c), they indicate the fluctuation $\overline{(\lambda C T_o)_f}$. Values of other parameters: $\lambda_- = 1$; $\Phi_C^{\text{top}} = -0.5$; $\langle \mathcal{X} \rangle = -0.1$; $\epsilon = 1/5$.

has been used for advancement in time [35,36]. A snapshot of the fields C and T_o is shown Fig. 4.

The production term λ is defined following Refs. [11,13],

$$\lambda_- \equiv \lambda_{T_o<0} = \epsilon^{-1} \lambda_{T_o>0}. \tag{68}$$

One of the motivations for this choice is that Eq. (68) provides a source of fluctuations analogous to those which could be expected, presumably, from taking into account the finite-size spectrum of the crystals.

As control parameters for the simulations we take λ_-, ϵ, Φ_C^{top}, and $\langle \mathcal{X} \rangle$. We concentrate on the three cases $\lambda_- = 1$, $\lambda_- = 0.1$, and $\lambda_- = 0.02$, which would correspond for $u_* = 0.01$ m/s to crystal radii $R \approx 0.14$ mm, $R \approx 0.45$ mm, and $R \approx 1$ mm [37]. We take $\epsilon = 1/50$ for the largest crystal

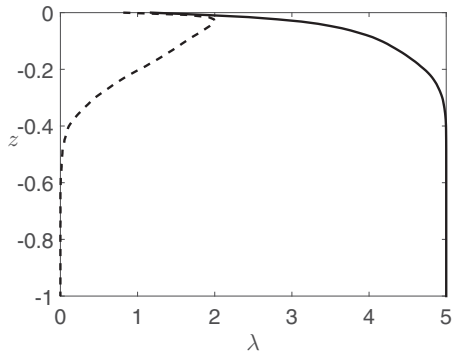

FIG. 6. Vertical profile of λ. Average solid; rms dashed. Values of the parameters $\lambda_- = 1$; $-\Phi_C^{\text{top}} = \langle \mathcal{X} \rangle = 0.1$; $\epsilon = 1/5$.

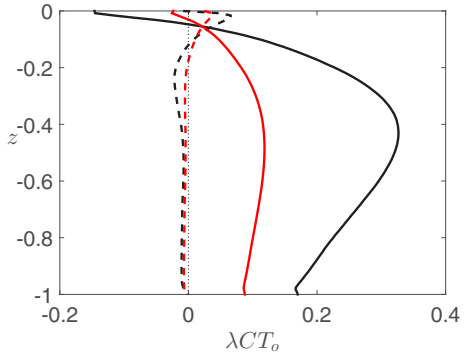

FIG. 8. Same as Fig. 7 for different values of ϵ and λ. $\lambda_- = 0.02$, $\epsilon = 1/50$ in red; $\lambda_- = 1$, $\epsilon = 1/5$ in black.

and $\epsilon = 1/5$ for the smaller ones, in accordance with the observations in Ref. [31]. The case $\epsilon = 1$ is also considered to evaluate the contribution to fluctuations from sources others than the growth-melt asymmetry in Eq. (68).

We put $\bar{u}_x(z) = 0$, as inclusion of a nonzero horizontal mean velocity profile has been observed to produce negligible effects on the dynamics. As done in Sec. VII, we put $\mathbf{u}_r = 0$, which is appropriate for the smallest crystals, but may be a rough approximation for the largest ones (see Fig. 1).

We note that ice may be present at the bottom of the domain, $z = \pm 1$, thus generating spurious ice fluxes. To evaluate the effect on the dynamics, we compare with the case in which an ice sink Φ_C^B is artificially added at $z = \pm 1$, with $\Phi_{T_o}^B \to \Phi_{T_o}^B + \Phi_C^B$, to guarantee conservation of $\langle \mathcal{X} \rangle$ (with a slight abuse of notation we are using superscript B for the bottom of the numerical domain although the region is not ice free). As shown in Fig. 5, the dynamics is modified only in the boundary layer region near $z = \pm 1$, the curves being essentially indistinguishable in the rest of the domain. We thus expect that the dynamics is properly taken into account by the model for generic values of the parameters.

As a general rule, we find that the fluctuation contribution to the production term $\overline{(\lambda C T_o)_f} = \overline{\lambda C T_o} - \bar{\lambda}\bar{C}\bar{T}_o$ is small, even though the rms components of the individual fields C, T_o, and λ are not small at all. We see in Figs. 5(b) and 5(c) that ice production fluctuations are concentrated around the transition region from negative to positive T_o. We see in Fig. 6 that fluctuations in λ concentrate roughly in the same region, which suggests that a strong contribution to the ice production fluctuations comes from the difference in melting and freezing rates described in Eq. (17).

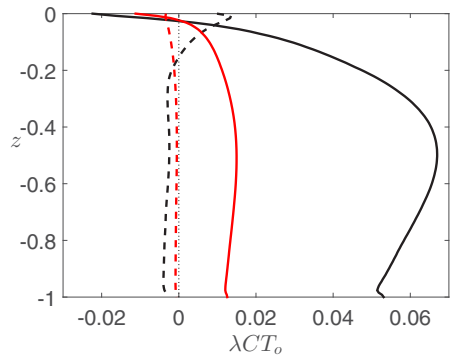

FIG. 7. Vertical profiles of the ice production for different values of ϵ. $\epsilon = 1$ in red, $\epsilon = 1/5$ in black; mean-field contribution $\bar{\lambda}\bar{C}\bar{T}_o$ solid line, fluctuation contribution $\overline{(\lambda C T_o)_f}$ dashed line. Values of the other parameters: $\lambda_- = -\Phi_C = \langle \mathcal{X} \rangle = 0.1$.

To determine the effect of the fluctuations of λ on the dynamics, we compare the case of frazil crystals with $\epsilon = 1$ and $\epsilon = 1/5$. We do not consider the contribution to fluctuations from the dependence of λ on the crystal distribution, which remains undetermined in a description based on the integrated field $C(\mathbf{r},t)$. We observe in Fig. 7 that for $\epsilon = 1$, $\overline{(\lambda C T_o)_f} = \lambda \tilde{\tilde{C}} \tilde{\tilde{T}}_o < 0$, suggesting a picture in which fluctuations of CT_o arise from cold water parcels rich in ice transported by turbulence from $z = 0$ into the body of the domain. As shown in Figs. 5(c), 7, and 8, for $\epsilon < 1$, fluctuations and mean-field components give contribution to ice production of opposite sign in most of the domain.

Fluctuations become negligible deeper in the column, where melting is dominant. This tells us that the mean-field analysis in the previous section may be appropriate for the decay of C [see Eq. (60)], but not for that of $\bar{T}_o$, due to the fluctuations of λ in the regions where $\bar{T}_o \to 0$ and therefore T_o undergoes most changes of sign.

IX. CONCLUSION

We have studied the process of ice formation in a turbulent, horizontally homogeneous stationary water column, as a balance of fluxes of heat, salinity, and ice. The following are our main results.

Imposing supercooling decrease with depth has allowed us to derive lower bounds on the ratio of sensible and latent heat fluxes to the atmosphere, which contain important information on the process of ice formation in the water column.

The minimum sensible heat flux ranges from roughly 1/2 to a few percents of the total flux depending on the strength of ice entrainment. The sensible heat in excess to the lower bound may be associated with ice melting at the bottom of the layer, or with direct heat transfer to the atmosphere, depending on whether a sufficiently thick grease ice layer is present or not at the water surface.

In the presence of entrainment, the minimum sensible heat flux accounts for the heat from the bottom of the column

required to melt the entrained ice crystals. The same amount of heat is released at the surface during ice formation. Entrained frazil ice behaves like a sort of conveyor belt for the heat, providing a contribution to the total flux, which, depending on the level of entrainment, may be comparable to the latent heat contribution from net ice production.

We have derived mean-field analytical expressions for the vertical profiles of salinity, temperature, and ice concentration in the limit of low entrainment, assuming the presence of a wind-induced mechanical boundary layer at the top of the water column.

It appears that, except in situations in which all of the water column is well above freezing, and entrainment is so low that the entrained ice completely melts, frazil ice fluxes reaching the bottom of the mechanical turbulent layer are present. At the same time, supercooled conditions can be found at substantial depth in the water column, confirming observations in the laboratory [17], in field campaigns [7,38,39], and in numerical simulations [16].

We explain the symmetric possibility of supercooling and frazil ice presence deep in the column, with the existence of a single reacting field actually being affected by ice formation [the field $\mathcal{Y}$ in Eq. (49)]. This has the consequence that the dynamics of supercooling and ice concentration, in the two cases in which one of the fields is small, are essentially identical.

We explain the observation that frazil ice and supercooling may be present at substantial depth in the water column with the smallness of the growth or melting rate of the ice crystals compared to the rate of turbulent mixing [the parameter λ in Eq. (52)]. The depths (normalized to the haline Obukhov depth) of the supercooled region in the presence of large frazil ice amounts, and of the frazil ice region in above-freezing conditions, are both $\sim\lambda^{-1}$.

We stress that all the above results on ice dynamics in the mechanical boundary layer are conditioned to smallness of the ratio of the rate of entrainment of frazil ice to total ice production [the parameter $\mathcal{E}$ in Eq. (29)]. It is not clear whether our results would be confirmed in the presence of strong entrainment, in which case, turbulence stabilization by frazil ice may may lead to a double-convection regime.

The mean-field results are confirmed by numerical analysis by means of a two-dimensional Kraichnan model. The analysis shows that a strong contribution to fluctuation is produced when asymmetry between the rates of ice formation and melting is assumed, as done in Refs. [12,13]; otherwise, fluctuations are small. This suggests that more accurate descriptions of ice formation, in which the size spectrum of the crystals and the different growth and melting rates of the different size classes are taken into account, could lead to similar higher fluctuation levels.

ACKNOWLEDGMENTS

This research was supported by FP7 EU project ICE-ARC (Grant agreement No. 603887), by MIUR-PNRA, PANACEA project (Grant No. 2013/AN2.02), and by COST Action grant MP1305.

[1] S. Martin, Frazil ice in rivers and oceans, Ann. Rev. Fluid Mech. **13**, 379 (1981)

[2] A. Alam and J. A. Curry, Evolution of new ice and turbulent fluxes over freezing winter leads, J. Geophys. Res. **103**, 15783 (1998).

[3] M. J. Doble, M. D. Coon, and P. Wadhams, Pancake ice formation in the Weddell Sea, J. Geophys. Res. **108**, C3209 (2003).

[4] H. Eicken, J. Kolatschek, J. Freitag, F. Lindemann, H. Kassen, and I. Dimitrenko, A key source area and constraints on entrainment for basin-scale sediment transport by Arctic sea ice, Geophys. Res. Lett. **27**, 1919 (2000).

[5] L. H. Smedsrud, Frazil ice entrainment of sediment: Large tank laboratory experiments, J. Glaciol. **47**, 461 (2001).

[6] S. F. Daly, Evolution of frazil ice in natural water bodies. in International Association for Hydraulic Research Working group on Thermal Regimes: Report on Frazil Ice, edited by S. F. Daly, US Army Cold Regions Research and Engineering Laboratory, Hanover, New Hampshire, 1994, p. 11.

[7] M. Ito *et al.*, Observations of supercooled water and frazil ice formation in an Arctic coastal polynya from moorings and satellite imagery, Ann. Glaciol. **56**, 307 (2015).

[8] A. Omstedt and U. Svensson, Modeling supercooling and ice formation in a turbulent Eckman layer, J. Geophys. Res. **89**, 735 (1984).

[9] A. Omstedt, Modeling frazil ice and grease ice formation in the upper layers of the ocean, Cold Reg. Sci. Technol. **11**, 87 (1998).

[10] U. Svensson and A. Omstedt, Simulation of supercooling and size distribution in frazil ice dynamics, Cold Reg. Sci. Technol. **22**, 221 (1994).

[11] A. Jenkins and A. Bombosch, Modeling the effects of frazil ice crystals on the dynamics and thermodynamics of ice shelf water plumes, J. Geophys. Res. **100**, 6967 (1995).

[12] L. H. Smedsrud and A. D. Jenkins, Frazil ice formation in an ice shelf water plume, J. Geophys. Res. **109**, C03025 (2004).

[13] P. R. Holland and D. L. Feltham, Frazil dynamics and precipitation in a water column with depth dependent supercooling, J. Fluid Mech. **530**, 101 (2005).

[14] B. K. Galton-Fenzi, J. R. Hunter, R. Coleman, S. J. Marsland, and R. C. Warner, Modeling the basal melting and marine ice accretion of the Amery Ice Shelf, J. Geophys. Res. **117**, C09031 (2012).

[15] E. D. Skyllingstad and D. W. Dembo, Turbulence beneath sea ice and leads: a coupled sea ice/large eddy simulation study, J. Geophys. Res. **106**, 2477 (2001).

[16] Y. Matsumura and K. I. Ohshima, Lagrangian model of frazil ice in the ocean, Ann. Glaciol. **56**, 373 (2015).

[17] S. Ushio and M. Wakatsuchi, A laboratory study of supercooling and frazil ice production processes in winter coastal polynias, J. Geophys. Res. **98**, 20321 (1993).

[18] S. Maus and S. De la Rosa, Salinity and solid fraction of frazil and grease ice, J. Glaciol. **58**, 594 (2012).

[19] L. H. Smedsrud and R. Skogseth, Field measurements of Arctic grease ice properties and processes, Cold Reg. Sci. Technol. **44**, 171 (2006).

[20] J. Bauer and S. Martin, A model of grease ice growth in small leads, J. Geophys. Res. **88**, 2917 (1983).
[21] D. L. Feltham, N. Untersteiner, J. S. Wettlaufer, and M. G. Worster, Sea ice is a mushy layer, Geophys. Res. Lett. **33**, L14501 (2006).
[22] J. P. Gosink and T. E. Osterkamp, Measurements and analyses of velocity profiles and frazil ice-crystals rise velocities during periods of frazil ice formation in rivers, Ann. Glaciol. **4**, 79 (1983).
[23] T. Fujioka and R. F. Sekerka, Morphological stability of disk crystals, J. Crystal Growth **24-25**, 84 (1974).
[24] L. Hammar and H. T. Shen, Frazil evolution in channels, J. Hydraul. Res. **33**, 291 (1995); P. R. Holland, D. L. Feltham, and S. Daly, On the Nusselt number for frazil ice growth a correction to Frazil evolution in channels by Lars Hammar and Hung-Tao Shen, *ibid.* **45**, 421 (2007).
[25] D. W. Rees Jones and A. J. Wells, Solidification of a disk-shaped crystal from a weakly supercooled binary melt, Phys. Rev. E **92**, 022406 (2015).
[26] W. Shimada and Y. Furukawa, Pattern formation of ice crystals during free growth in supercooled water, J. Phys. Chem. B **101**, 6171 (1997).
[27] In order for a flux-gradient relation between Φ_{T_o} and T_o to hold, it is necessary that T and S are transported together, which is reasonable if molecular diffusion can be disregarded.
[28] S. Martin and P. Kauffman, A field and laboratory study of wave damping by grease ice, J. Glaciol. **27**, 283 (1981).
[29] We are assuming that the microscopic flows in the ice layer are produced by mechanical means, such as wave stirring and wind-induced shear motions. Linearity in T and S could be violated by convection at the crystal scale.
[30] S. Leibovich, The form and dynamics of Langmuir circulation, Ann. Rev. Fluid Mech. **15**, 391 (1983).
[31] T. R. Ghobrial, M. R. Loewen, and F. E. Hicks, Characterizing suspended frazil ice in rivers using upward looking sonars, Cold Regions Sci. Technol. **86**, 113 (2013).
[32] C. M. Bender and S. A. Orszag, *Advanced Mathematical Methods for Scientists and Engineers*. (McGraw-Hill, New York, 1979).
[33] R. H. Kraichnan, Small-scale structure of a scalar field convected by turbulence, Phys. Fluids **11**, 945 (1968).
[34] G. Falkovich, K. Gawedzki, and M. Vergassola, Particles and fields in fluid turbulence, Rev. Mod. Phys. **73**, 913 (2001).
[35] D. Elhmaidi, A. Provenzale, and A. Babiano, Elementary topology of two-dimensional turbulence from a Lagrangian viewpoint and single-particle dispersion, J. Fluid Mech. **257**, 533 (1993).
[36] D. Elhmaidi, J. von Hardenberg, and A. Provenzale, Dissipation and Filament Instability in Two-Dimensional Turbulence, Phys. Rev. Lett. **95**, 014503 (2005).
[37] We are assuming for γ the parametrization in Ref. [24]. The alternative parametrization in Refs. [23,25] would lead to values of R larger by a factor $\approx$3.3.
[38] R. Skogseth, F. Nilsen, and L. H. Smedsrud, Supercooled water in an Arctic polynya: Observations and modeling, J. Glaciol. **55**, 43 (2009).
[39] I. A. Dmitrenko *et al.*, Observations of supercooling and frazil ice formation in the Laptev Sea coastal polynya, J. Geophys. Res. Oceans **115**, C05015 (2010).